Polar methane accumulation and rain storms on Titan from simulations of the methane cycle

T. Schneider[1], S. D. B. Graves[1], E. L. Schaller[2] & M. E. Brown[1]

[1]*California Institute of Technology, Pasadena, California 91125, USA*

[2]*NASA Dryden Aircraft Operations Facility, National Suborbital Education and Research Center, Palmdale, CA 93550, USA*

Titan has a methane cycle akin to Earth's water cycle, with lakes in polar regions[1,2], preferentially in the north[3], dry low latitudes with fluvial features[4,5] as well as occasional rain storms[6,7], and tropospheric clouds mainly (so far) in southern midlatitudes and polar regions[8–15]. Previous models have explained the low-latitude dryness as a result of atmospheric methane transport into middle and high latitudes[16]. Not hitherto explained is why lakes are found only in polar regions and preferentially in the north, how low-latitude rain storms arise, and why clouds cluster in southern middle and high latitudes. Here we report simulations with a 3D atmosphere model coupled to a dynamic methane surface reservoir. We find that methane is cold-trapped and accumulates in polar regions, preferentially in the north because the northern summer, at aphelion, is longer and has greater net precipitation. The net precipitation in polar regions is balanced in the annual mean by slow along-surface methane transport toward midlatitudes and subsequent evaporation. In low latitudes, rare but intense storms occur around the equinoxes, producing enough precipitation to carve surface features. Tropospheric clouds form primarily in middle and high latitudes of the summer hemisphere (until recently the southern). We predict that in the north polar region,

prominent clouds will form within $\sim$2 years and lake levels will rise over the next $\sim$15 years.

Explanations for Titan's tropospheric clouds range from control by local topography and cryovolcanism[11,12] to control by a seasonally varying global Hadley circulation with methane condensation in its ascending branch[8,17]. General circulation models (GCMs) have suggested that clouds either form primarily in midlatitudes and near the poles in both hemispheres[18], inconsistent with the observed hemispheric differences[14], or that they form where insolation is maximal[17], likewise not fully consistent with newer observations[14,15]. Similarly, explanations for the polar hydrocarbon lakes range from control by local topography and a subsurface methane table[2] to control by evaporation and precipitation, which depend on the atmospheric circulation[16,19]. GCMs have suggested that surface methane accumulates near the poles, but also in midlatitudes[16], where no lakes have been observed, and without the observed hemispheric asymmetry. No model has reproduced the latitudinal distribution of surface methane including its hemispheric asymmetry, is fully consistent with the cloud distribution, or has shown intense enough precipitation in low latitudes to carve fluvial features. Indeed, it has been suggested that the atmosphere is too stable for rain storms to occur in low latitudes[20]. Yet intense and, at least in one case, apparently precipitating storms have been observed[6,7].

We investigate the extent to which major features of Titan's climate and methane cycle can be explained by large-scale processes using a GCM that includes an atmosphere model with a methane cycle and surface reservoir. The atmosphere model is 3D, in contrast to previous 2D models[16–18], because the intermittency of clouds and features such as equatorial superrotation[21] (impossible in axisymmetric circulations[22]) point to the importance of 3D dynamics. The surface

reservoir gains or loses methane according to the local rates of precipitation (P) and evaporation (E), with horizontal diffusion as a simple representation of slow surface flows from moister to drier regions. We show zonal and temporal averages from a simulation in a statistically steady state, which does not depend on initial conditions except for the (conserved) total methane amount initially in the atmosphere-surface system (here, 12 m liquid methane in the global mean). See Supplementary Information for details.

In the statistically steady state, the annual- and global-mean methane concentration in the atmosphere corresponds to 7 m liquid methane—possibly somewhat higher than but broadly consistent with observations[23,24]; the remainder is at the surface. Methane has accumulated near the poles (Fig. 1a). It is transported there from spring into summer by a global Hadley circulation (Fig. 1b), with ascent (Fig. 2) and a precipitation maximum (Fig. 1c) over the summer pole. Some of the methane accumulating near the summer pole flows along the surface (on Titan possibly also below the surface[2]) toward midlatitudes. It evaporates again and is transported back toward the opposite pole when the circulation reverses around equinox. Polar regions lose methane from late summer through winter, with zonal-mean net evaporation rates ($E-P$) reaching $\sim 0.2\,\mathrm{m\,yr^{-1}}$ (1 yr referring to 1 Earth year) in southern summer (Fig. 1b). This is consistent with observations: the zonal-mean evaporative loss rate is of similar magnitude as (but smaller than) the recently observed local drop in south polar lake levels[25]. We predict that the north polar region will gain methane for the next ~ 15 years, with zonal-mean net precipitation rates ($P-E$) reaching $\sim 1.4\,\mathrm{m\,yr^{-1}}$ around NSS (Fig. 1b). This should lead to an observable rise in lake levels.

Methane is cold-trapped at the poles. Along with annual-mean insolation, annual-mean evap-

oration is minimal near the poles. (Evaporation is the dominant loss term in the surface energy balance and scales with insolation.) Surface temperatures decrease from low latitudes to the poles throughout the year (Fig. 1d), because almost all solar energy absorbed there is used to evaporate methane. At the same time, precipitation is maximal near the summer pole (Fig. 1c) because the insolation maximum destabilizes the atmosphere with respect to moist convection. This can be seen from the moist static energy (MSE), which measures more directly than temperature the energetic effect of solar radiation on the atmosphere, as only net radiation at the top of the atmosphere drives the vertically integrated MSE balance if, as is the case on Titan and in our GCM, the surface heat capacity is negligible[26]; similarly, insolation variations are the dominant driver of variations in the MSE balance integrated over the planetary boundary layer. Indeed, along with insolation, near-surface MSE is maximal near the summer poles (Fig. 1e). This implies a propensity for deep convection because the slow rotation and large thermal inertia of Titan's atmosphere constrain horizontal and temporal temperature and MSE variations above the boundary layer to be weak[27], and the vertical MSE stratification controls convective stability (MSE increasing with altitude indicates stability)[26]. Lower latitudes, by contrast, do not favor deep convection although they are warmer than the summer poles because their maximal insolation is weaker, and hence their maximal near-surface MSE is also lower (Fig. 1e). The result is the drying of lower latitudes and the accumulation of methane at the poles, similar to what has been suggested previously but without methane accumulation in midlatitudes[16] (see Supplementary Information for possible reasons for this difference).

However, although low latitudes are dry and have smaller mean precipitation rates than the

poles (Fig. 1c), the precipitation intensity is largest in low latitudes (Fig. 1f); that is, low-latitude rain storms are rare but intense. Precipitation rates in the more intense storms are of similar magnitude ($\gtrsim 10\,\mathrm{mm\,day^{-1}}$) as rough estimates of the rates needed to carve the observed fluvial surface features[4,28]. The precipitation intensity is largest before and around the equinoxes, when the reversal of the Hadley circulation (cf. Fig. 1b) is associated with dynamic instabilities. The waves they generate are sufficiently strong to occasionally trigger deep convection and intense rain if they advect relatively moist air from higher latitudes over the warm low latitudes. This contrasts with 2D and local models that suggest intense precipitation does not occur in low latitudes[16–18,20]. But it is consistent with the observations of intense and apparently precipitating low-latitude storms on Titan[6,7].

In the GCM as on Titan[3], there is more surface methane in polar regions in the north than in the south (Fig. 1a). This asymmetry is a robust result irrespective of initial conditions (e.g., whether methane is initially in the atmosphere or at the surface). It is caused by Saturn's orbital eccentricity, which leads to a northern summer (currently around aphelion) that is longer and cooler than the southern, and therefore allows more methane to be cold-trapped. Although the maximal rate of net precipitation (Fig. 1b) is greater in the warmer southern summer, polar net precipitation integrated over a Titan year is greater in the north primarily because its rain season is longer. For example, averaged over the polar caps bounded by the polar circles ($63.3°$ N/S), the period during which absorbed insolation exceeds $0.5\,\mathrm{W\,m^{-2}}$ is 14% longer in the north than in the south; annually integrated net precipitation is $0.86\,\mathrm{m}$ (38%) greater in the north, $0.76\,\mathrm{m}$ of which attributable to increased precipitation and $0.10\,\mathrm{m}$ to decreased evaporation. (The contribution of evaporation to

the hemispheric asymmetry is small because it scales with insolation, which, in the annual mean, is equal in the north and south; this contradicts a previous hypothesis that the hemispheric asymmetry were due to evaporation differences[3].) Because in the annual mean, the excess net precipitation in polar regions is balanced by along-surface methane transport toward midlatitudes and subsequent evaporation, surface methane extends farther equatorward in the north than in the south (Fig. 1a), as on Titan[3]. Thus, surface or subsurface transport of methane is essential for maintaining a statistically steady state with nonzero net precipitation in polar regions and asymmetries between the hemispheres; we expect that such transport occurs on Titan. One reason why previous models[16] did not produce hemispheric asymmetries is because they were lacking a representation of this transport.

Our GCM also reproduces the observed tropospheric methane cloud distribution (Fig. 3). For the period with detailed observations since 2001, the GCM reproduces the observed prevalence of clouds in the southern hemisphere mid-latitudes and polar region and the decreasing frequency of south polar clouds since 2005 (Fig. 3a)[6,13–15]. For the same period, the GCM indicates a lack of clouds in the northern hemisphere, consistent with observations with ground-based telescopes[6,13] and the Cassini VIMS instrument[14]. Observations with the Cassini ISS instrument[15] indicate more frequent northern-hemisphere clouds (Fig. 3a), but these appear to be lake-effect clouds owing to stationary zonal inhomogeneities in topography and the lake distribution[29], which are not captured in the GCM. The relative frequency of clouds in the GCM fits observations better than previous 2D models[16–18]. A 3D model that resolves waves and instabilities in the atmosphere is essential for reproducing the non-sinusoidal seasonal variations of cloudiness.

Deep convective clouds in the GCM form not only above the polar near-surface MSE maximum but also in the summer hemisphere midlatitudes (Fig. 2). There they form above relatively high surface temperatures (Fig. 1d), which destabilize the boundary layer with respect to dry convection. This occasionally leads to moist convection and mean ascent in the free troposphere (above shallow boundary-layer circulation cells), resulting in a secondary cloud frequency maximum above the boundary layer (Fig. 2). The surface reservoir underneath these clouds is depleted ($\lesssim 7\,\mathrm{cm}$ depth in the mean, see Fig. 1a), consistent with the observed lack of lakes in mid-latitudes[2]. We predict that, with the reversal of the Hadley circulation in spring, north polar clouds will emerge within $\sim$2 yrs , earlier than suggested by other models[17], and should be clearly observable for $\sim$10 yrs; around NSS, prominent cloudiness may extend into midlatitudes (Fig. 3b). The validity of our predictions of seasonal changes will soon be testable as Titan's northern hemisphere spring proceeds into summer and new observations become available.

1. Stofan, E. *et al.* The lakes of Titan. *Nature* **445**, 61–64 (2007).

2. Hayes, A. *et al.* Hydrocarbon lakes on Titan: Distribution and interaction with a porous regolith. *Geophys. Res. Lett.* **35**, L09204 (2008). Doi:10.1029/2008GL033409.

3. Aharonson, O. *et al.* An asymmetric distribution of lakes on Titan as a possible consequence of orbital forcing. *Nature Geosci.* **2**, 851–854 (2009).

4. Lebreton, J. *et al.* An overview of the descent and landing of the Huygens probe on Titan. *Nature* **438**, 758–764 (2005).

5. Lorenz, R. *et al.* The sand seas of Titan: Cassini RADAR observations of longitudinal dunes. *Science* **312**, 724–727 (2006).

6. Schaller, E. L., Roe, H. G., Schneider, T. & Brown, M. E. Storms in the tropics of Titan. *Nature* **460**, 873–875 (2009).

7. Turtle, E. P. *et al.* Rapid and extensive surface changes near Titan's equator: Evidence of April showers. *Science* **331**, 1414–1417 (2011).

8. Brown, M. E., Bouchez, A. H. & Griffith, C. A. Direct detection of variable tropospheric clouds near Titan's south pole. *Nature* **420**, 795–797 (2002).

9. Porco, C. C. *et al.* Imaging of Titan from the Cassini spacecraft. *Nature* **434**, 159–168 (2005).

10. Griffith, C. A. *et al.* The evolution of Titan's mid-latitude clouds. *Science* **310**, 474–477 (2005).

11. Roe, H. G., Bouchez, A. H., Trujillo, C. A., Schaller, E. L. & Brown, M. E. Discovery of temperate latitude clouds on Titan. *Astrophys. J.* **618**, L49–L52 (2005).

12. Roe, H. G., Brown, M. E., Schaller, E. L., Bouchez, A. H. & Trujillo, C. A. Geographic control of Titan's mid-latitude clouds. *Science* **310**, 477–479 (2005).

13. Schaller, E. L., Brown, M. E., Roe, H. G., Bouchez, A. H. & Trujillo, C. A. Dissipation of Titan's south polar clouds. *Icarus* 517–523 (2006).

14. Brown, M. E., Roberts, J. E. & Schaller, E. L. Clouds on Titan during the Cassini prime mission: A complete analysis of the VIMS data. *Icarus* **205**, 571–580 (2010).

15. Turtle, E. P. *et al.* Seasonal changes in Titan's meteorology. *Geophys. Res. Lett.* **38**, L03203 (2011).

16. Mitchell, J. The drying of Titan's dunes: Titan's methane hydrology and its impact on atmospheric circulation. *J. Geophys. Res* **113**, E08015 (2008).

17. Mitchell, J. L., Pierrehumbert, R. T., Frierson, D. M. W. & Caballero, R. The dynamics behind Titan's methane clouds. *Proc. Nat. Acad. Sci.* **103**, 18421–18426 (2006).

18. Rannou, P., Montmessin, F., Hourdin, F. & Lebonnois, S. The latitudinal distribution of clouds on Titan. *Science* **311**, 201–205 (2006).

19. Mitri, G., Showman, A. P., Lunine, J. I. & Lorenz, R. D. Hydrocarbon lakes on Titan. *Icarus* **186**, 385–394 (2007).

20. Griffith, C. A., McKay, C. P. & Ferri, F. Titan's tropical storms in an evolving atmosphere. *Astrophys. J.* **687**, L41–L44 (2008).

21. Flasar, F. M., Baines, K. H., Bird, M. K., Tokano, T. & West, R. A. Atmospheric dynamics and meteorology. In Brown, R. H., Lebreton, J.-P. & Waite, J. H. (eds.) *Titan from Cassini-Huygens*, chap. 13, 323–352 (Springer, 2009).

22. Schneider, T. The general circulation of the atmosphere. *Ann. Rev. Earth Planet. Sci.* **34**, 655–688 (2006).

23. Penteado, P. F., Griffith, C. A., Greathouse, T. K. & de Bergh, C. Measurements of CH_3D and CH_4 in Titan from infrared spectroscopy. *Astrophys. J.* **629**, L53–L56 (2005).

24. Tokano, T. *et al.* Methane drizzle on Titan. *Nature* **442**, 432–435 (2006).

25. Hayes, A. *et al.* Transient surface liquid in Titan's polar regions from Cassini. *Icarus* **211**, 655–671 (2011).

26. Neelin, J. D. & Held, I. M. Modeling tropical convergence based on the moist static energy budget. *Mon. Wea. Rev.* **115**, 3–12 (1987).

27. Charney, J. G. A note on large-scale motions in the tropics. *J. Atmos. Sci.* **20**, 607–609 (1963).

28. Perron, J. T. *et al.* Valley formation and methane precipitation rates on Titan. *J. Geophys. Res.* **111**, E1001 (2006).

29. Brown, M. E. *et al.* Discovery of lake-effect clouds on Titan. *Geophys. Res. Lett.* **36**, L01103 (2009).

30. Jennings, D. E. *et al.* Titan's surface brightness temperatures. *Astrophys. J.* **691**, L103–L105 (2009).

Acknowledgements We are grateful for support by a NASA Earth and Space Science Fellowship and a David and Lucile Packard Fellowship. We thank Ian Eisenman for code for the insolation calculations and Oded Aharonson, Alex Hayes, and Alejandro Soto for helpful comments on a draft. The simulations were performed on Caltech's Division of Geological and Planetary Sciences Dell cluster.

Author Contributions T.S. and M.E.B conceived the study; T.S., S.B.G., and E.L.S. developed the GCM. E.L.S. and M.E.B. provided data; and T.S. and S.B.G. wrote the paper, with contributions and comments from all authors.

Competing Interests The authors declare that they have no competing financial interests.

Correspondence Correspondence and requests for materials should be addressed to T. Schneider. (email: tapio@caltech.edu).

Figure 1: Annual cycle of zonal-mean climate statistics in Titan GCM. The lower time axes start at autumnal equinox (corresponding to November 1995); the upper axes indicate corresponding calendar years. Solid grey lines are contours of absorbed solar radiation at the surface (contour interval $0.25\,\mathrm{W\,m^{-2}}$), and dashed grey lines mark the northern and southern summer solstices (NSS and SSS). **a** Methane surface reservoir depth (colorscale truncated at 20 cm). **b** Net evaporation ($E - P$) at the surface (colors, contour interval $0.1\,\mathrm{mm\,day^{-1}}$, with $1\,\mathrm{day} = 86400\,\mathrm{s}$) and column-integrated meridional methane flux (arrows, with the longest corresponding to a flux of $5.4\,\mathrm{kg\,m^{-1}\,s^{-1}}$). The methane flux is largely accomplished by the mean meridional (Hadley) circulation; eddy fluxes are a factor $\gtrsim 3$ weaker and strongest in middle and low latitudes. **c** Precipitation rate. **d** Surface temperature. The surface temperatures are roughly consistent with observations[30], with similar equator-pole temperature contrasts and with a winter pole that is $\sim$1 K colder than the summer pole. (Generally, tropospheric temperatures in the simulation are within 1 K of Titan observations; see Supplementary Fig. S2.) **e** Moist static energy per unit volume averaged between surface and 2 km altitude. MSE is the sum of gravitational potential energy and moist enthalpy, including the contribution of the latent heat of methane vapor[26]. **f** Precipitation intensity (precipitation rate when it rains). The precipitation intensity is the mean precipitation conditional on the precipitation rate being nonzero (exceeding $10^{-3}\,\mathrm{mm\,day^{-1}}$). All fields are averages over longitude and time (25 Titan years) in the statistically steady state of a simulation with a total of 12 m liquid methane in the atmosphere-surface system. The statistically steady state was reached a in long (135 Titan years) spin-up period. Although the GCM climate is statistically zonally symmetric, climate statistics such as the methane surface reservoir depth exhibit instantaneous zonal asymmetries ("lakes"), which can persist for several Titan years.

Figure 2: Relation between tropospheric cloudiness and atmospheric circulation in southern summer. Colors show the tropospheric methane cloud frequency and contours the streamfunction of the mean meridional mass circulation, at 9.1 yrs past autumnal equinox (corresponding to January 2005, the time of the Huygens landing on Titan). The contouring is logarithmic, with factors of $\sqrt{2}$ and 2 between adjacent contour levels for cloud frequency and streamfunction, respectively. Solid streamfunction contours for clockwise rotation, dashed contours for counterclockwise rotation (contour levels at $\pm 2^{-1}, 1, 2, 2^2, \cdots \times 10^9\,\mathrm{kg\,s^{-1}}$). The cloud frequency is the relative frequency of phase changes of methane on the grid scale and in the convection scheme of the GCM. Moist convection and maxima in cloud frequency above the boundary layer occur above the polar near-surface MSE maximum and above relatively high surface temperatures in midlatitudes (here, at $\sim 30^\circ$S) in the summer hemisphere. (Moist convection rarely occurs above the local surface temperature maximum in the winter hemisphere (here, at 15°–30°N) because this lies under the descending branch of the Hadley circulation, where the free troposphere is relatively dry.)

Figure 3: Annual cycle of tropospheric methane cloud frequency. **a** Focusing on the time period for which detailed observations are available or will be available soon, cloud frequency in GCM and cloud observations. The GCM cloud frequency (colors) is a mass-weighted vertical average of the cloud frequency (Fig. 2) in the troposphere, between the surface and 32 km altitude. Brown circles represent ground-based cloud observations[13], magenta lines Cassini Visual and Infrared Mapping Spectrometer (VIMS) observations[14], and light magenta lines Cassini Imaging Science Subsystem (ISS) observations[15]. The bars across the top indicate the time period over which the observations were made. (However, the coverage of VIMS and ISS observations is not continuous,

so a lack of VIMS and ISS cloud observations in the periods indicated by the bars does not necessarily mean clouds were in fact absent.) Solid grey lines are contours of absorbed solar radiation at the surface, as in Fig. 1. **b** As in **a**, except over a complete Titan year, beginning at autumnal equinox, and excluding observations.

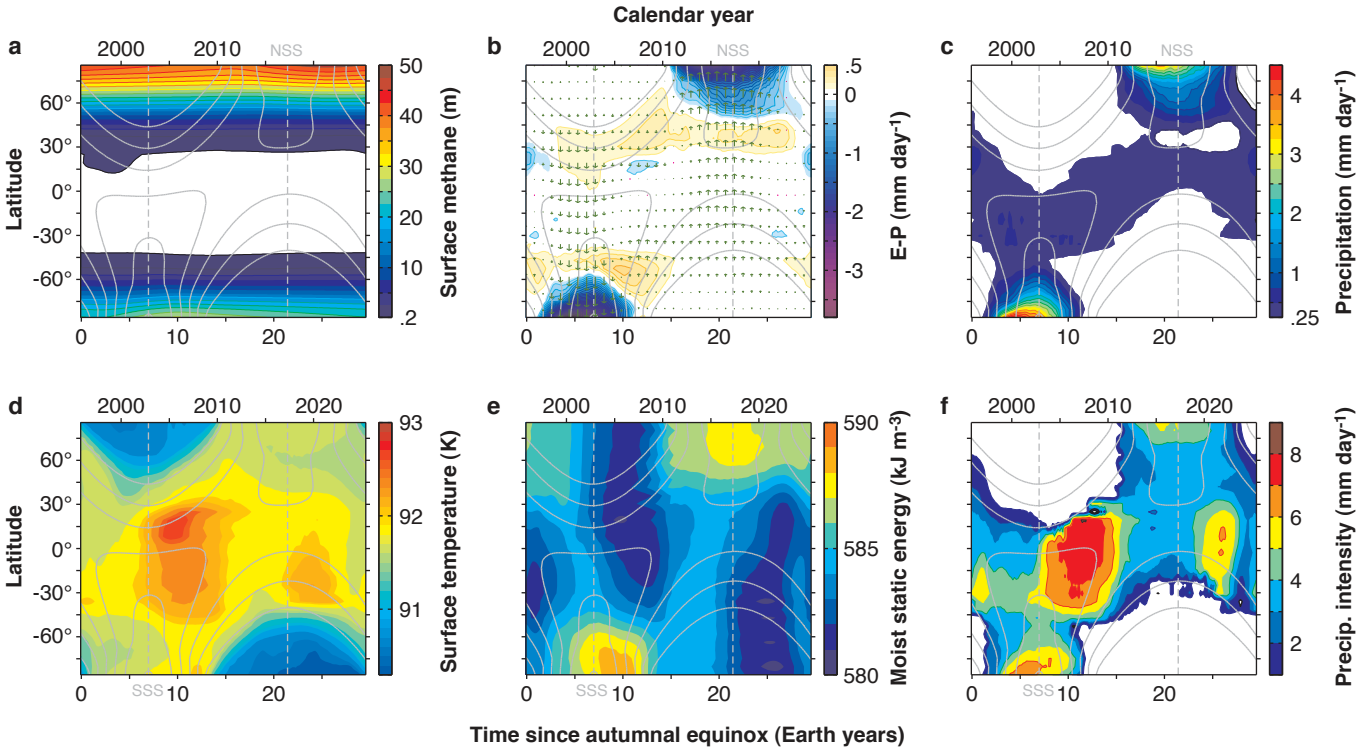
Calendar year
a
b
c
d
e
f
2000
2010
2020
NSS
SSS
60°
30°
0°
-30°
-60°
Latitude
0
10
20
50
40
30
20
10
.2
Surface methane (m)
.5
0
-1
-2
-3
E-P (mm day-1)
4
3
2
1
.25
Precipitation (mm day-1)
93
92
91
Surface temperature (K)
590
585
580
Moist static energy (kJ m-3)
8
6
4
2
Precip. intensity (mm day-1)
Time since autumnal equinox (Earth years)

Fig. 1

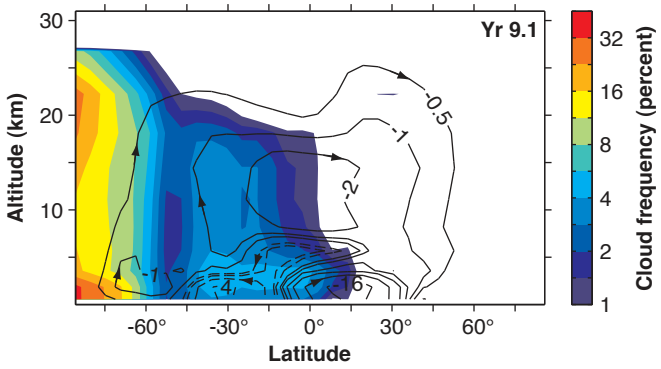
Yr 9.1
Altitude (km)
30
20
10
-60°
-30°
0°
30°
60°
Latitude
-0.5
-1
-2
-1
-4
-16
32
16
8
4
2
1
Cloud frequency (percent)

Fig. 2

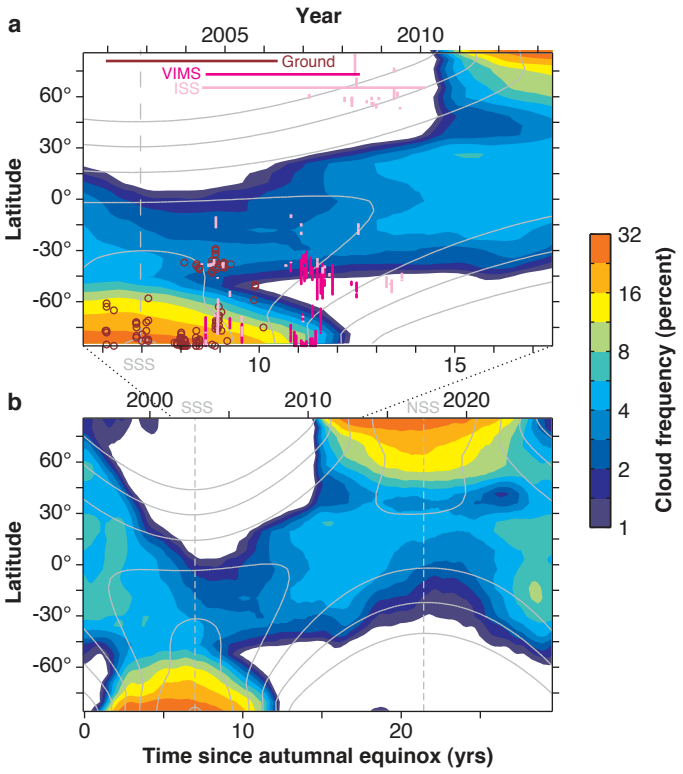
a
Year
2005
2010
Ground
VIMS
ISS
60°
30°
0°
-30°
-60°
Latitude
SSS
10
15
b
2000
SSS
2010
NSS
2020
60°
30°
0°
-30°
-60°
Latitude
0
10
20
Time since autumnal equinox (yrs)
32
16
8
4
2
1
Cloud frequency (percent)

Fig. 3

Supplementary Information

Our GCM is based on the Flexible Modeling System of the Geophysical Fluid Dynamics Laboratory (http://fms.gfdl.noaa.gov). It is similar to standard models for Earth's atmosphere, but with Titan's radius, planetary rotation rate, material properties, and seasonally varying insolation, and with a methane cycle instead of a water cycle. The GCM has similarities to the models in refs. 16, 17, but unlike those, it is 3D and eddy-resolving and has a different representation of radiative transfer and surface processes.

Resolution. The GCM solves the hydrostatic primitive equations in vorticity-divergence form, using the spectral transform method in the horizontal and finite differences in the vertical[31]. The horizontal spectral resolution is T21 (corresponding to about $5^\circ \times 5^\circ$ resolution of the transform grid). The vertical coordinate is $\sigma = p/p_s$ (pressure p normalized by surface pressure p_s); it is discretized with 18 unequally spaced levels[32]. The top of the model is at $\sigma = 0$; the uppermost full level has a mean pressure of 15 mbar (altitude $\sim$90 km). The time-stepping scheme is a semi-implicit leapfrog scheme (timestep 1600 s).

Methane thermodynamics. Methane is advected with a finite-volume scheme on the transform grid. A large-scale condensation scheme ensures that the mean relative humidity in a grid cell does not exceed 100% relative to saturation over a binary methane-nitrogen mixture (saturation vapor pressure 10600 Pa at 90.68 K)[33]. Condensing methane precipitates, and condensate on the grid scale re-evaporates into the air it falls through until that air is saturated. Only the vapor-liquid phase transition is considered, and the latent heat of vaporization is taken to be constant

($L = 4.9 \times 10^5\,\mathrm{J\,kg^{-1}}$), as in refs. 16, 17, 34 (that is, methane freezing is neglected). The latent heat is smaller than that for pure methane to approximately take its reduction for a binary methane-nitrogen mixture into account[33]. Thermodynamic effects of ethane on the mixture[35] are not explicitly taken into account.

Moist convection. A quasi-equilibrium convection scheme[36] represents moist convection. It is adapted for methane thermodynamics, takes the effects of methane on the air density into account[34], and relaxes convectively unstable atmospheric columns on a timescale of 4 hrs toward a moist pseudoadiabat with a relative humidity of 70%.

This is an idealized representation of moist convection. Like other quasi-equilibrium moist convection schemes, it likely underestimates precipitation rates in extreme events; however, mean precipitation rates (which are more strongly energetically constrained) are likely more adequately simulated[37].

Radiative transfer. Radiative transfer is represented using the two-stream approximation. It assumes an atmosphere with horizontally homogeneous composition and with wavelength-independent transfer of solar radiation and thermal radiation, ignoring poorly constrained processes such as cloud-radiative feedbacks. Saturn's seasonally varying insolation is imposed at the top of atmosphere, taking into account the current orbital configuration (eccentricity, obliquity, and longitude of perihelion); we ignore diurnal insolation variations because the large thermal inertia of the atmosphere is expected to strongly damp diurnal temperature variations.

Solar radiation is scattered and absorbed in the atmosphere, assuming diffuse incidence and multiple scattering[38], with asymmetry factor 0.65 and single-scattering albedo 0.95. The solar extinction optical depth is specified as

$$\tau_s = \tau_{s0}(p/p_0)^\gamma,$$

with optical thickness $\tau_{s0} = 5$ at $p_0 = 1.467\times10^5$ Pa and empirical exponent $\gamma = 0.21$. The surface albedo is 0.3 uniformly, implying a planetary Bond albedo of 0.20 given the radiative transfer prescription and its parameters. The parameters are chosen to approximate optical properties of the surface[39] and of atmospheric aerosols[40] and to give a good fit to measured solar radiative fluxes; within our GCM domain, they imply net solar radiative fluxes that are within 6% of those measured by the Huygens probe[41] (Supplementary Fig. S1).

Thermal radiation is absorbed in the atmosphere, with an optical depth

$$\tau_l = \tau_{l0}\left[\alpha(p/p_0)^2 + (1-\alpha)(p/p_0)\right]$$

that roughly represents a mixture of collision-induced absorption (quadratic term, weight $\alpha = 0.85$) and absorption by a well-mixed absorber (linear term, weight $1-\alpha = 0.15$). The thermal optical thickness of the atmosphere is $\tau_{l0} = 10$ (cf. ref. 42).

In the statistically steady state of the GCM, this formulation of radiative transfer results in a realistic temperature profile with a tropopause, without the need to invoke discrete haze layers or cloud decks; in the lower troposphere, temperatures are within l K and near the tropopause within $\sim$5 K of those measured by the Huygens probe[43] (Supplementary Fig. S2).

Boundary layer. A k-profile scheme represents boundary-layer turbulence[44]. Surface fluxes of momentum, sensible heat, and methane (where available) are calculated using standard bulk aerodynamic formulae, with exchange coefficients determined from Monin-Obukhov similarity theory, a roughness length of $5 \times 10^{-3}\,\mathrm{m}$, and an additive gustiness term of $0.1\,\mathrm{m\,s^{-1}}$ in surface velocities to represent subgrid-scale wind fluctuations. (In the bulk aerodynamic formula for methane fluxes, we do not use an additional "methane availability parameter" as in some other studies[17,45].) Our results are not sensitive to the choice of these parameters.

Subgrid-scale dissipation. Horizontal ∇^8 hyperdiffusion in the vorticity, divergence, temperature, and specific humidity equations represents unresolved turbulent dissipation. The hyperdiffusion coefficient is chosen to give a damping time scale of 3 hrs at the smallest resolved scale. (Sufficient subgrid-scale dissipation is essential for the robustness of our results. Simulations with insufficient subgrid-scale dissipation of specific humidity resulted in grid-scale noise and surface methane reservoirs with large variations across narrow latitude bands, similar to what is seen in simulations in ref. 16; these were numerical artifacts.) In the uppermost model layer, horizontal diffusion damps vorticity and divergence variations (diffusivity $5 \times 10^7\,\mathrm{m^2\,s^{-1}}$).

Surface reservoir. Surface methane hydrology is represented by a simplified bucket model[46]. Where surface methane is available, the evaporation rate is given by the bulk aerodynamic formula; where none is available, the evaporation rate vanishes. The surface methane level in each grid cell increases or decreases according to the local rates of precipitation and evaporation. Additionally, methane diffuses along the surface (diffusivity $100\,\mathrm{m^2\,s^{-1}}$), as a simple representation of relatively slow surface flows.

Surface energy balance. The surface temperature evolves according to the surface energy balance of a homogenous slab with heat capacity $2.5 \times 10^5\,\mathrm{J\,m^{-2}\,K^{-1}}$ (similar to that of a porous icy regolith[47]) , with temperature tendencies balanced by insolation, thermal radiative fluxes, and the surface fluxes of sensible heat and latent heat (methane evaporation). The value of the slab heat capacity does not substantially affect our results, as long as it is much smaller than the heat capacity of the atmosphere ($\sim 10^8\,\mathrm{J\,m^{-2}\,K^{-1}}$).

Initialization, simulations, and parameter sensitivity. We carried out simulations with various ways of initializing the atmosphere and surface methane reservoir (adding small random perturbations in the atmosphere to break the axisymmetry of the initial state). The simulation described in the main paper was initialized with a dry surface and with an isothermal (86 K) atmosphere containing the equivalent of 12 m of liquid methane distributed uniformly. The total amount of methane in the atmosphere-ocean system is (up to small numerical inaccuracies) conserved in the GCM. We obtained a statistically steady state in a long spin-up period (135 Titan years, with 1 Titan year = 10758 Earth days)—much longer than those used in previous studies[16–18,45]. The results we show are averages over 25 Titan years in the statistically steady state.

Our central results are insensitive to how the simulations are initialized, provided a statistically steady state is reached (which, depending on the initial condition, can take $\gtrsim 100$ Titan years because of the small net precipitation differences between the hemispheres). For example, a simulation initialized with a dry isothermal atmosphere and with 12 m of methane uniformly at the surface eventually produces a statistically steady state that is indistinguishable from that of the simulation described in the main paper. With less than $\sim$7 m of methane initially, the surface

dries out completely, as in ref. 16; with somewhat more methane initially, the southern methane reservoir is only seasonally filled. Generally, with more methane initially, more accumulates at the poles, and the equatorward extent of the polar reservoirs increases, but the amount of methane in the atmosphere does not increase substantially beyond $\sim$7 m. The equatorward extent of the polar reservoirs also increases with the along-surface diffusivity. However, the formation of polar reservoirs is a robust result that occurs with a variety of methane amounts and diffusivities.

While our GCM reproduces the observed surface temperature distribution[30] and tropospheric vertical temperature profile (Fig. S2) relatively well, it only reproduces qualitative aspects of the zonal wind distribution. For example, it does produce equatorial superrotation, as is observed[21], but the tropospheric zonal winds are generally weaker than those observed (up to 2–3 $\mathrm{m\,s^{-1}}$ in the upper troposphere of the GCM vs. over 10 $\mathrm{m\,s^{-1}}$ inferred from the Huygens descent[21]). We will discuss the wind structure and the underlying dynamics in more detail elsewhere.

Supplemental References

31. Durran, D. R. *Numerical Methods for Wave Equations in Geophysical Fluid Dynamics*, vol. 32 of *Texts in Applied Mathematics* (Springer, New York, 1999).

32. Simmons, A. J. & Burridge, D. M. An energy and angular-momentum conserving vertical finite-difference scheme and hybrid vertical coordinates. *Mon. Wea. Rev.* **109**, 758–766 (1981).

33. Thompson, W. R., Zollweg, J. A. & Gabis, D. H. Vapor-liquid equilibrium thermodynamics of N2 + CH4: Model and Titan applications. *Icarus* **97**, 187–199 (1992).

34. O'Gorman, P. A. & Schneider, T. The hydrological cycle over a wide range of climates simulated with an idealized GCM. *J. Climate* **21**, 3815–3832 (2008).

35. Graves, S. D. B., McKay, C. P., Griffith, C. A., Ferri, F. & Fulchignoni, M. Rain and hail can reach the surface of Titan. *Planet. Space Sci.* **56**, 346–357 (2008).

36. Frierson, D. M. W. The dynamics of idealized convection schemes and their effect on the zonally averaged tropical circulation. *J. Atmos. Sci.* **64**, 1959–1976 (2007).

37. Sun, Y., Solomon, S., Dai, A. & Portmann, R. W. How often does it rain? *J. Climate* **19**, 919–934 (2006).

38. Petty, G. W. *A First Course in Atmospheric Radiation* (Sundog Publishing, Madison, Wisconsin, 2006), 2nd edn.

39. Schröder, S. E. & Keller, H. U. The reflectance spectrum of Titan's surface at the Huygens landing site determined by the descent imager/spectral radiometer. *Planet. Space Sci.* **56**, 753–769 (2008).

40. Tomasko, M. G. & West, R. A. Aerosols in Titan's atmosphere. In Brown, R. H., Lebreton, J.-P. & Waite, J. H. (eds.) *Titan from Cassini-Huygens*, chap. 12, 297–321 (Springer, 2009).

41. Tomasko, M. *et al.* Heat balance in Titan's atmosphere. *Planet. Space Sci.* **56**, 648–659 (2008).

42. McKay, C. P., Pollack, J. B. & Courtin, R. The greenhouse and antigreenhouse effects on Titan. *Science* **253**, 1118–1121 (1991).

43. Fulchignoni, M. *et al.* In situ measurements of the physical characteristics of Titan's environment. *Nature* **438**, 785–791 (2005).

44. Troen, I. B. & Mahrt, L. A simple model of the atmospheric boundary layer: Sensitivity to surface evaporation. *Boundary-Layer Met.* **37**, 129–148 (1986).

45. Tokano, T. Impact of seas/lakes on polar meteorology of Titan: Simulation by a coupled GCM-sea model. *Icarus* **204**, 619–636 (2009).

46. Manabe, S. Climate and the ocean circulation: I. The atmospheric circulation and the hydrology of the earth's surface. *Mon. Wea. Rev.* **97**, 739–773 (1969).

47. Tokano, T. Meteorological assessment of the surface temperatures on Titan: Constraints on the surface type. *Icarus* **173**, 222–242 (2005).

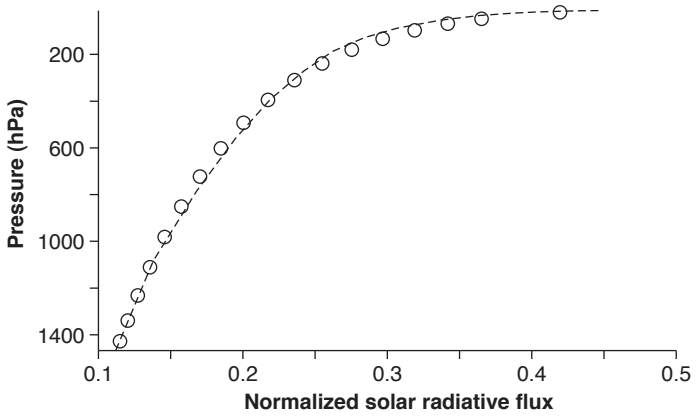

Figure S1: Net solar radiative flux normalized by the incident flux at the top of the atmosphere in GCM and measured on Titan. Dashed line: Solar radiative flux inferred from Descent Imager/Spectral Radiometer data obtained by the Huygens probe[41]. (The flux is interpolated from altitude to pressure levels using data obtained by the Huygens Atmospheric Structure Instrument[43].) Circles: Solar radiative flux at the vertical coordinate levels in the GCM. In the GCM, the normalized solar radiative flux is spatially and temporally constant; only the incident flux at the top of the atmosphere varies with latitude and time.

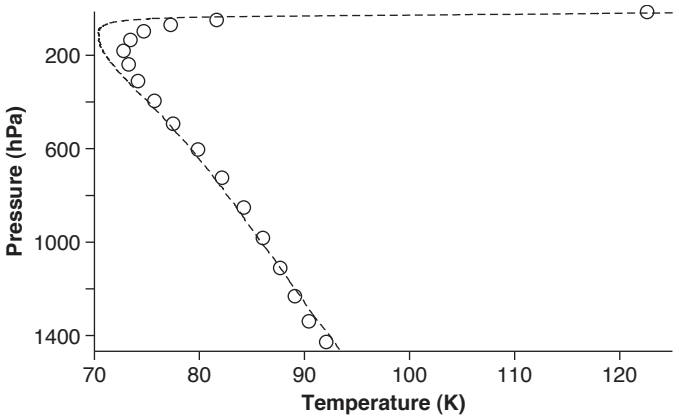

Figure S2: Thermal structure at Huygens landing site in GCM and measured on Titan. Dashed line: Temperature measured by the Huygens Atmospheric Structure Instrument at 10.2°S on 14-January-2005[43]. Circles: Mean temperature at the corresponding latitude and time (9.1 yrs past autumnal equinox) at the vertical coordinate levels of the GCM.